Long Period Grating Imprinted on a Flat-Shaped Plastic Optical Fiber for Refractive Index Sensing

Yuan LIU[1], Yanfei ZHOU[1], Haiyang BAO[2], and Jie ZHENG[1*]

[1]*State Key Laboratory of Integrated Optoelectronics, College of Electronic Science and Engineering, Jilin University, Changchun 130012, China*

[2]*Changchun Institute of Optics, Fine Mechanics and Physics, Chinese Academy of Sciences, Changchun 130012, China*

[*]Corresponding author: Jie ZHENG E-mail: zhengjie@jlu.edu.cn

Abstract: A corrugated surface long period grating (LPG) was fabricated on a flat-shaped plastic optical fiber (POF) as a refractive index (RI) sensor by a simple pressing with the heat pressure and mechanical die press print method. The light propagation characteristics of an LPG imprinted on a multi-mode POF were analyzed by the method of geometrical optics. Theoretical and experimental results showed that the structural parameters of the sensor affected the RI sensing performance, and the sensor with a thinner flat thickness, a deeper groove depth of the corrugated surface LPG, and a longer LPG exhibited better RI sensing performance. When the POF with a diameter of 1 mm was pressed with the heat pressure to a flat shape with a thickness of 600 μm, an LPG with a period of 300 μm, a groove depth of 200 μm, and a length of 6 cm was fabricated on it, and the RI sensitivity of 1447%/RIU was obtained with a resolution of 5.494×10^{-6} RIU. In addition, the influences of the POF cladding, tilting of LPG, and bending of the sensing structure were investigated. The results demonstrated that after removing the cladding and tilting or bending the LPG, the RI sensing performance was improved. When the LPG imprinted on the flat-shaped POF was bent with a curvature radius of $6/\pi$ cm, the highest sensitivity of 6 563%/RIU was achieved with a resolution of 2.487×10^{-9} RIU in the RI range of 1.3330–1.4230. The proposed sensor is a low-cost solution for RI measurement with the features of easy fabrication, high sensitivity, and intensity modulation at the visible wavelengths.

Keywords: Plastic optical fiber; fiber optic sensor; flat-shaped optical fiber; long period grating; refractive index sensing

Citation: Yuan LIU, Yanfei ZHOU, Haiyang BAO, and Jie ZHENG, "Long Period Grating Imprinted on a Flat-Shaped Plastic Optical Fiber for Refractive Index Sensing," *Photonic Sensors*, 2023, 13(4): 230416.

1. Introduction

Fiber optic sensing, rapidly developed alongside the fiber communication technology, has multiple benefits over electrical sensors including the high sensitivity, immunity to electromagnetic interference, flexibility, corrosion resistance, light weight, and remote operation [1]. The applications range from temperature, liquid level, strain, environment, and displacement detection to PH sensing and bending measurement [2–9].

Refractive index (RI) is one of the most important physical constants. Physical quantities such as concentration, pH value, and oxygen content of substances can be reflected by RI measurement

Received: 10 April 2023 / Revised: 6 June 2023

DOI: 10.1007/s13320-023-0691-z
Article type: Regular

[10]. Its measurement finds applications in diverse fields, including substance identification, the control of food quality [11], and biochemical sensing fields [12]. Over the years, fiber optic RI sensors have gained much attention among researchers. Different kinds of fiber optic RI sensors have been developed on the basis of the fiber Bragg grating [13], optical fiber surface plasmon resonance [14], fiber long period grating (LPG) [15], and interferometric fiber optic sensors [16], etc. However, these sensors, which are primarily based on mode glass optical fibers (GOFs), are difficult to fabricate and require complex processing of the fibers. RI sensors based on plastic optical fibers (POFs) have gained attention due to their unique advantages over GOFs, including the large diameter, high numerical aperture, and low attenuation in the visible region. Furthermore, the POFs are more flexible and have lower softening temperature, allowing for easier structural modification. Due to their multi-mode characteristic, the POFs based sensors are well-suited for low-cost intensity modification schemes, making them a valuable alternative to the traditional technology [17].

It is well known that modifying the POFs' structural parameters are often required to enhance the RI sensitivity [17]. There are a variety of structural modification methods, such as tapering [18], macro-bending [19], side-polishing [20], multi-notched [21], imprinting LPG [22, 23], twisting POF [24], and screw-shaped POF [25].

For the periodic modification of the multi-mode POFs, C. X. Teng *et al*. [21] utilized a multi-notched POF as an RI sensor and achieved a sensitivity of 1130%/RIU. Actually, the multi-notched POF was a coarsely corrugated surface LPG with a large period. P. Xue *et al*. improved the LPG fabricating technique and utilized a corrugated surface LPG imprinted on a POF [22] and a D-shaped POF [23] for an RI sensing purpose, respectively. Within the RI range of 1.33–1.45, the LPG inscribed on the POF demonstrated the highest sensitivity of 2 815%/RIU. For the LPG imprinted on the D-shaped POF case [23], an extremely high RI sensitivity of 9786%/RIU was reached in a higher RI range of 1.40–1.45, but in a lower RI range of 1.33–1.40, the sensitivity was just 2676%/RIU. In addition, the both works [22, 23] demonstrated that imprinting the LPG on a thin POF results in the superior RI sensing performance over those on the thick POF.

In this paper, we tried a different way to modify the structure of the POF for improving the RI sensing performance. By the use of a thick commercial POF (CK-40, Super Eska, with a diameter of 1 mm), we thinned the POF in one-dimension and then imprinted an LPG on it. Thus, a corrugated surface LPG imprinted on a flat-shaped POF was proposed as an RI sensor, which was mainly made by the following two steps: the POF was firstly pressed with the heat pressure to form a flat-shaped POF, then, an LPG was imprinted on the surface of the obtained flat-shaped POF by the method of the simple mechanical die press print. By changing and optimizing the structural parameters of the LPG imprinted on the flat-shaped POF, the RI sensing performances of the obtained sensor were evaluated and improved experimentally.

2. Fabrication and principle

2.1 Fabrication of an LPG imprinted on a flat-shaped POF

The commercial step-index POFs (Super Eska) with the polymethyl methacrylate (PMMA) core and fluorinated polymer cladding were used in this work to fabricate the flat-shaped POF and the LPG on it. The parameters of the POF are listed in Table 1.

Table 1 Parameters of the POF.

Fiber category	Diameter (mm)	Diameter of the core (mm)	RI of the core	RI of the cladding
CK-10	1000	980	1.492	1.402

An LPG imprinted on a flat-shaped POF was fabricated by pressing with the heat pressure and

simple mechanical die press print method, as shown in Figs. 1(a)–1(d). To achieve a flat-shaped POF, the POF was initially placed on a sample holding platform and clamped between two heated metal molds with flat surfaces, as illustrated in Fig. 1(a). The temperature of the molds was roughly 60 ℃. Then, the controlled pressure F was perpendicularly applied to the metal molds and continuously pressed on the POF for a few seconds. Consequently, a cylindrical POF was deformed into a flat-shape, as shown in Fig. 1(b). The obtained flat-shaped POF was fixed on a sample holding platform, then, a metal mould with a periodic V-groove structure was pressed on the POF in the way that the mould was perpendicular to the fiber axial. Keeping the state for a few seconds, the V-groove structure could be transferred onto the POF, and the corrugated surface LPG was formed, as shown in Fig. 1(c). Among them, the period of the metal mould was 300 μm. After that, an LPG imprinted on a flat-shaped POF was formed, as shown in Fig. 1(d). The thickness (d) of the flat-shaped structure could be adjusted by applying the pressure. The width of the periodic V-grooved structure on the mould determined the length (L) of the LPG. In the same way, the pressure could be used to adjust the groove depth (h).

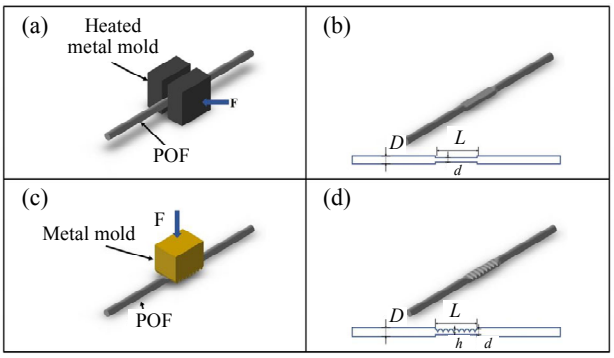

Fig. 1 Fabrication process of the LPG imprinted on the flat-shaped POF: (a) schematic of fabricating the flat-shaped POF by the pressing with the heat pressure, (b) schematic of the flat-shaped POF, where L, d, and D are the length, thickness, and diameter of the flat-shaped POF, (c) schematic of fabricating an LPG imprinted on the flat-shaped POF by a mechanical die-press-print method, and (d) schematic of the LPG imprinted on the flat-shaped POF, where h is the groove depth of the LPG.

2.2 Principle

2.2.1 Propagation of light in an LPG imprinted on a multi-mode POF

According to the LPG theory, the optical power transmitted through the fiber as core modes at a wavelength λ, is coupled between core modes and cladding modes at the grating region. This coupling process can be expressed as

$$\lambda = (n_{\text{co eff}} - n_{\text{cl eff}})\Lambda \tag{1}$$

where Λ is the period of the gratings, and $n_{\text{co eff}}$ and $n_{\text{cl eff}}$ are the effective RIs of core modes and cladding modes, respectively. Since in single-mode fibers only one core mode and many cladding modes exist, the core-cladding coupling occurs at certain specific wavelengths. However, in the case of a multi-mode fiber with a large number of core modes and cladding modes, the core-cladding power coupling occurs at all wavelengths and the wavelength dependence is not resolved.

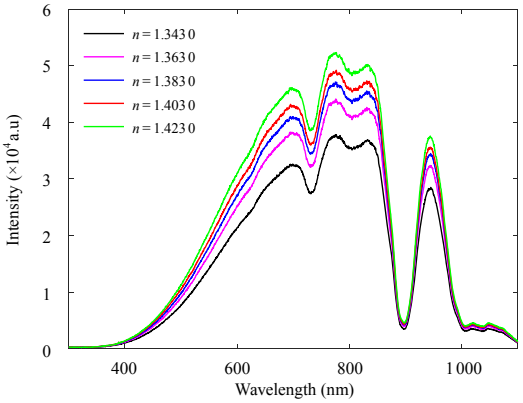

Fig. 2 Transmission spectra of the flat-shaped POF with an LPG in measured liquids with different RIs, where the POF diameter is 1 mm, the thickness of the flat-shaped structure is 600 μm, the LPG length is 2 cm, the period is 300 μm, and the groove depth is 200 μm.

A transmission spectra measurement was verified by the above mentions. A tungsten halogen source (HL-2000, Ocean Optics) was used as a light source, and the light was guided into a flat-shaped POF (with an LPG) in measured liquids with RIs of 1.333 0–1.423 0. An optical spectrum analyzer (Maya 2000, Ocean Optics) was used to detect the spectra. The transmission spectra of the LPG with a period length of 300 μm and a groove depth of

200 μm imprinted on the flat-shaped POF with a thickness of 600 μm and a length of 2 cm are shown in Fig. 2. It was found that there were not significant resonant wavelengths since the POFs were multi-mode fibers, and there were a large number of core modes and cladding modes, which resulted in a loss of the transmitted intensity taking place due to the mode coupling by the LPG. Therefore, the sensor was more suitable for intensity modulation instead of wavelength modulation schemes. The changes in the environmental RI would affect the mode coupling characteristics and lead to a loss of transmitted intensity changes, as shown in Fig. 2. Therefore, the principle of the operation for the sensor was based on the propagation losses introduced by the LPG imprinted on the flat-shaped POF, which were modulated by the environmental RIs.

2.2.2 Propagation loss introduced by an LPG imprinted on a multi-mode POF

The light propagation characteristics of an LPG imprinted on a multi-mode fiber were analyzed by the method of geometrical optics. In order to simplify the calculations, the following assumptions were introduced: 1) the light power distribution was uniform in the fiber, and the transmission losses were ignored because the sensor was short; (2) the structure of the LPG area was regular, and the surface of the V-groove was smooth.

A light source was modeled by the angular distribution of power from each of its elemental surface area dS. One elemental source is shown in Fig. 3, which emitted within a cone of half-angle θ. Light emitted at the angle θ_0 to the area dΩ, and the corresponding radiated power dP is given by [26][27]

$$\begin{aligned} \mathrm{d}P &= I_0 \cos\theta_0 \mathrm{d}S\mathrm{d}\Omega \\ &= I_0 \cos\theta_0 r\mathrm{d}r\mathrm{d}\varphi \sin\theta_0 \mathrm{d}\theta_0 \mathrm{d}\theta_\varphi \\ (0 &\leqslant \theta_0 \leqslant \theta) \end{aligned} \tag{2}$$

where I_0 is a constant, (θ_0, θ_φ) are spherical polar angles with respect to the incidence normal vector, and (r, φ) are polar coordinates relative to the fiber axis.

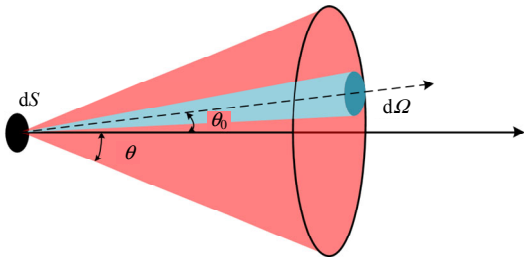

Fig. 3 Elemental source dS.

According to (2), the total power P_0 in the straight fiber was obtained by integrating dP over the complete ranges of values of r, φ, θ_0, and θ_φ. P_0 is expressed as the following:

$$\begin{aligned} P_0 &= T_0 I_0 \pi^2 (d/2)^2 \sin^2\theta_a \\ &= T_0 I_0 \pi^2 (d/2)^2 (n_{\mathrm{co}}^2 - n_{\mathrm{cl}}^2) \end{aligned} \tag{3}$$

where T_0 is Fresnel's transmission coefficient at the incident end of the fiber, d is the diameter of the fiber POF core, n_{co} is the RI of the fiber core, n_{cl} is the RI of the fiber cladding, and θ_a is the maximum angle of the incidence and satisfies

$$n_0 \sin\theta_a = n_{\mathrm{co}} \sin\theta_c \tag{4}$$

where n_0 is the RI of air (n_0=1), and θ_c is the cosine of the critical angle for the total reflection at the boundary core/cladding.

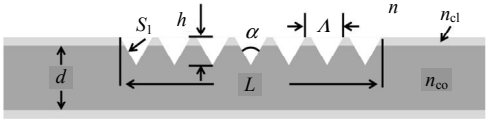

Fig. 4 Schematic diagram of the LPG which is imprinted on the cylindrical POF.

As shown in Fig. 4, by analogy with (3), the light leakage power P_1 from the first V-groove surface S_1 is

$$P_1 = \eta T_0 I_0 \pi S_1 \sin^2\theta_a (n_{\mathrm{co}}^2 - n^2)\cos(\alpha/2) \tag{5}$$

where η is the coupling coefficient, α is the V-groove angle, n is the environmental RI, and

$$S_1 = \frac{(d/2)^2 \arcsin^2 \dfrac{2\sqrt{d-h^2}}{d} - (d/2-h)\sqrt{dh-h^2}}{\cos(\alpha/2)}. \tag{6}$$

So, when the light passed through the first V-groove, the proportion of light leakage power γ is

$$\gamma = \frac{P_1}{P_0} = \frac{\eta S_1 \cos(\alpha/2)(n_{co}^2 - n^2)}{\pi (d/2)^2}. \quad (7)$$

As the V-grooves of the sensitive zone were mutually identical, so were the proportions of light leakage power at other V-grooves, and the normalized optical power P after the Nth grooves of the sensitive zone can be expressed as

$$P = (1-\gamma)^{\frac{L}{\Lambda}} \quad (8)$$

where L is the LPG length, and Λ is the LPG period.

Assuming that the coupling coefficient is 1 ($\eta = 1$), we calculated the variation of the relative transmission (normalized) power through the LPG with the core diameter d of the POF ($n_{co} = 1.492$), period Λ, groove depth h, and length L of the LPG according to (2)–(8) respectively, in the RI range of 1.3330–1.4530 as shown in Figs. 5(a)–5(d).

As shown in Fig. 5, the light power propagation in the LPG increased with an increase in the POF diameter and period of the LPG, decreased with an increase in the groove depth and length of the LPG, and increased with an increase in the environment RI inversely. The calculation results showed that a longer corrugated surface LPG with a shorter period and a deeper groove depth imprinted on a thinner POF would introduce a higher propagation loss, which indicated that the LPG owned a higher coupling efficiency in this case.

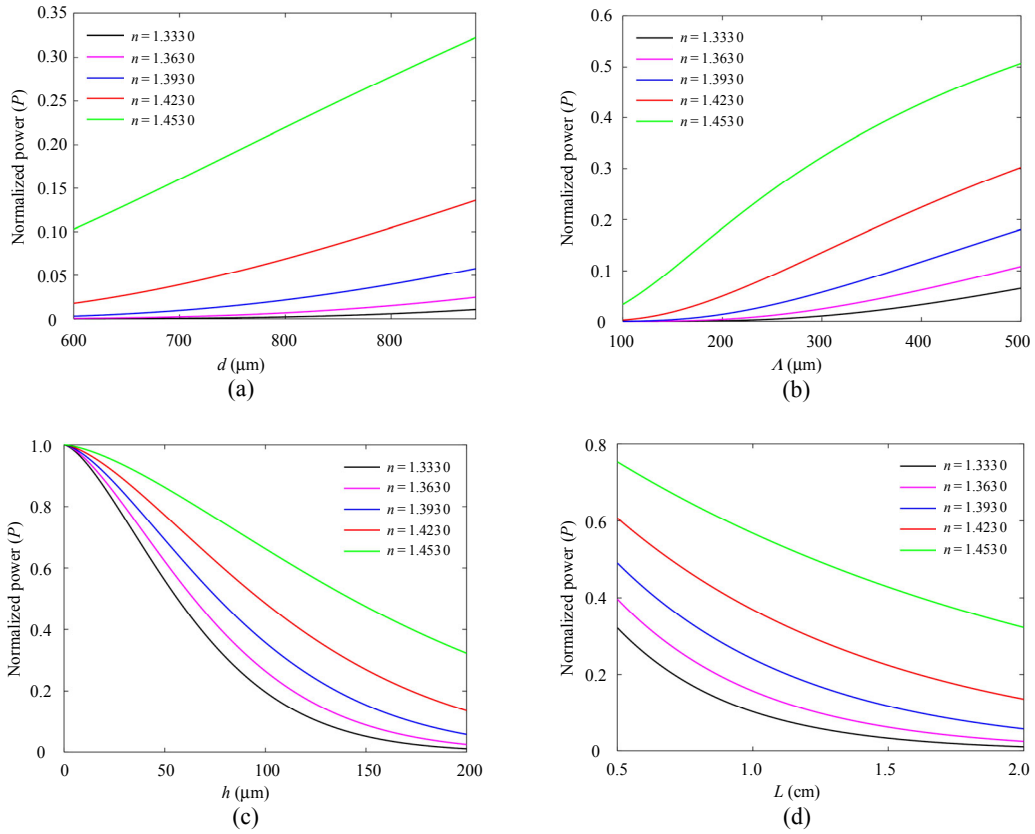

Fig. 5 Variation of light power (normalized) in an LPG imprinted on a POF ($n_{co} = 1.492$) with the (a) core diameter (d) of the POF ($L = 2$ cm, $h = 200$ μm, and $\Lambda = 300$ μm), (b) period (Λ) of the LPG ($L = 2$ cm, $h = 200$ μm, and $d = 980$ μm), (c) groove depth (h) of the LPG ($L = 2$ cm, $d = 980$ μm, and $\Lambda = 300$ μm), and (d) length (L) of the LPG ($d = 980$ μm, $h = 200$ μm, and $\Lambda = 300$ μm).

By the use of a POF with a large diameter of 1 mm, we thinned the diameter of a POF in one-dimension by pressing with the heat pressure method to form a flat-shaped POF, and then imprinted an LPG on it so as to achieve a similar effect to the preparation of the LPG on the small diameter POF. Due to the limitation of experimental conditions, only the LPG with a period of 300 μm

could be used for this work. By changing the structural parameters (the flat thickness, the groove depth of the corrugated surface LPG, and its length) of the LPG imprinted on the flat-shaped POF, the RI sensing performance of the obtained sensor would be evaluated experimentally.

3. RI sensing

The schematic of the experimental setup for RI measurement is shown in Fig. 6. The sensing probe was horizontally placed into the glycerin solution. One end of the flat-shaped POF with an LPG was connected with a laser source (TLS001-635, Thorlabs) with a wavelength of 635 nm and a launched power of 2 mW, and the other end was connected with a photodiode (S120C, Thorlabs) with a responsivity of 0.41 A/W and a resolution of 1 nW. The RI sensing performances of the sensor were tested by the deionized water and glycerol solutions with RIs of 1.323 0 to 1.423 0. The experiment was performed at the room temperature (20 ℃).

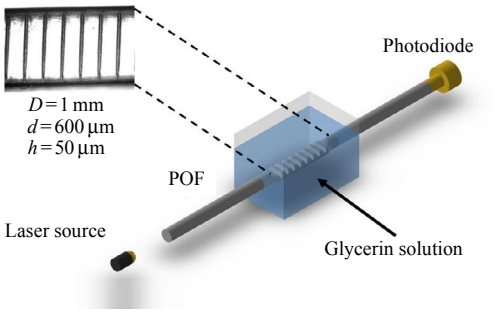

Fig. 6 Schematic diagram of the RI sensing experimental setup.

The LPG imprinted on the flat-shaped POF was immersed into the measured solutions. The transmittance T is equal to P_i/P_0, where P_i and P_0 are the average transmitted light intensities in measuring the glycerin solutions with different RIs ranging from 1.333 0 to 1.423 0 and the deionized water, respectively. The sensitivity (S) is expressed as the following [18]:

$$S(\%/\mathrm{RIU}) = \frac{\Delta T}{\Delta n} \times 100\% \tag{9}$$

where ΔT is the variation of the transmittance and Δn is the variation of RI. The resolution (R) is expressed as the following [18]:

$$R = \frac{3\delta}{S} \tag{10}$$

where δ is the standard deviation of the transmittance in measuring the blank sample (air).

The flat-shaped structure with the thicknesses of 600 μm, 700 μm, and 800 μm and a length of 2 cm was fabricated on the POF with a diameter of 1.00 mm. The RI sensing performances for the POF and the flat-shaped POFs with different thicknesses (d) were evaluated. The experimental results are shown in Fig. 7, in which the error bars arising from the fluctuations of the light source and the detector noises are shown for each data point, which represent the accidental error. They are given as the relative standard deviation.

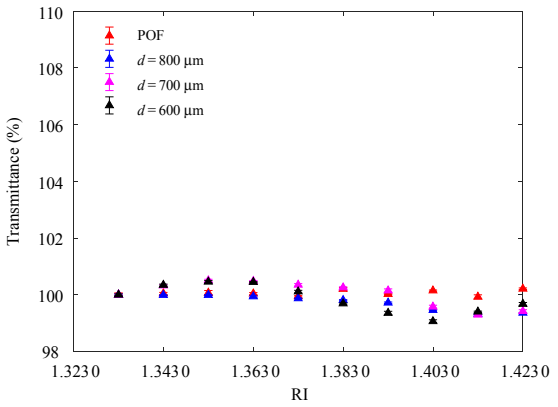

Fig. 7 RI sensing performances of the flat-shaped POFs with different thicknesses (d). The thicknesses (d) of flat-shaped POFs are 600 μm, 700 μm, and 800 μm, respectively, and the length is 2 cm.

As shown in Fig. 7, it showed that the POF with the flat-shaped structure had no obvious sensing performances, therefore, the LPGs with a period length of 300 μm and a groove depth of 50 μm imprinted on the flat-shaped POFs with different thicknesses of 600 μm, 700 μm, and 800 μm and the length of 2 cm were tested for the RI sensing performance, as shown in Fig. 8. For the LPGs imprinted on the flat-shaped POFs case, it could be observed that the transmittance was monotonically increased as the environmental RI increased. The results showed that the sensitivity increased as the

thickness of the flat structure decreased, which was similar to the simulation result in Fig. 5. When the thickness (d) of the flat-shaped structure was 600 μm, the RI sensitivity of the LPG imprinted on the flat-shaped POF reached 113.3%/RIU in the range of 1.3330–1.4230. The experimental results of the LPGs imprinted on the flat-shaped POFs with different thicknesses in Fig. 8 are listed in Table 2.

Table 2 Experimental results of LPGs with a period length of 300 μm imprinted on the flat-shaped POFs with different thicknesses in Fig. 8 (D = 1 mm, L = 2 cm, and h = 50 μm).

Thickness (μm)	δ	Sensitivity (%/RIU)	Resolution (RIU)	Correlation coefficient R^2
1 000	2.59×10^{-4}	33.19	2.341×10^{-3}	0.9748
800	4.58×10^{-4}	56.72	2.422×10^{-3}	0.9813
700	2.84×10^{-4}	86.48	9.852×10^{-4}	0.9923
600	3.48×10^{-4}	113.30	9.214×10^{-4}	0.9862

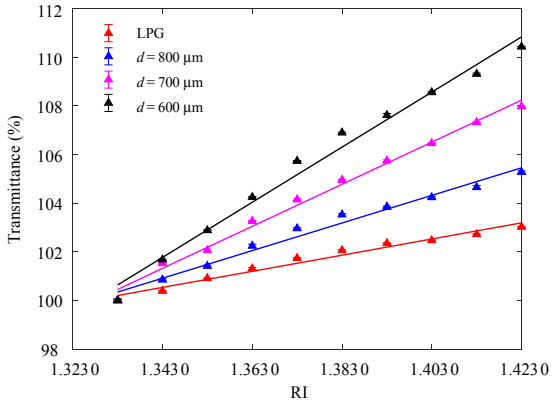

Fig. 8 RI sensing performances of the LPGs with a period length of 300 μm and a groove depth of 50 μm imprinted on the flat-shaped POFs with different thicknesses (d). The thicknesses (d) of flat-shaped POFs are 600 μm, 700 μm, and 800 μm, and the length is 2 cm.

Although the RI sensing performance was improved after imprinting an LPG on the POF, the sensitivity of the LPGs with a groove depth of 50 μm imprinted on the flat-shaped POFs was still relatively low. So, we tried to increase the groove depth (h) for the purpose of introducing more propagation losses. The groove depths of the LPGs changing from 50 μm to 200 μm imprinted on the flat-shaped POFs with a thickness of 600 μm and a length of 2 cm were tested, as shown in Fig. 9. It is found that the RI sensitivities of flat-shaped POFs assisted by LPGs were improved as the groove depths increased, which was due to that LPGs with a deeper groove depth could lead more guided modes leaking out to interact with the environment. The highest sensitivity of 450.7%/RIU was obtained when the groove depth was 200 μm. The results of LPGs with different depths imprinted on the flat-shaped POFs in Fig. 8 are listed in Table 3. It can be seen in Fig. 9 that the sensitivity of the sensor reached the maximum when the groove depth was 200 μm.

Table 3 Experimental results of LPGs with a period of 300 μm and different depths imprinted on the flat-shaped POFs in Fig. 9 (D = 1 mm, d = 600 μm, and L = 2 cm).

Groove depth (mm)	δ	Sensitivity (%/RIU)	Resolution (RIU)	Correlation coefficient R^2
50	3.48×10^{-4}	113.3	9.214×10^{-4}	0.9862
100	6.48×10^{-4}	157.2	1.237×10^{-5}	0.9833
150	1.72×10^{-4}	205.6	2.510×10^{-4}	0.9873
200	1.44×10^{-3}	450.7	9.585×10^{-4}	0.9959

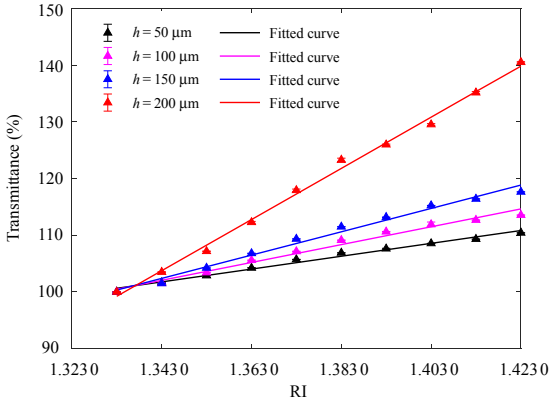

Fig. 9 RI sensing performances of LPGs with a period of 300 μm and a groove depth (h) changing from 50 μm to 200 μm imprinted on the flat-shaped POFs. The thickness (d) of flat-shaped structures on POFs is 600 μm.

Finally, we tried to increase the length (L) of the LPG for the purpose of introducing more propagation losses. The LPGs with a groove depth of 200 μm and different lengths from 2 cm to 6 cm imprinted on the flat-shaped POFs with a thickness of 600 μm were tested, as shown in Fig. 10. It was found that the RI sensitivities of LPGs imprinted on flat-shaped POFs were improved as the lengths of LPGs increased from 2 cm to 6 cm, which was due to that LPGs with a longer length could lead more guided modes leaking out to interact with the environment. The highest sensitivity of 1447%/RIU was obtained when the length of LPG was 6 cm. The results of the LPGs with different lengths imprinted

on the flat-shaped POFs in Fig. 10 are listed in Table 4.

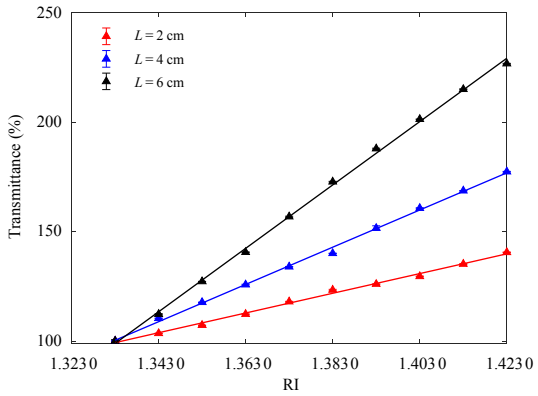

Fig. 10 RI sensing performances of the LPGs with a period of 300 μm and a groove depth of 200 μm. The length (L) changes from 2 cm to 6 cm imprinted on the flat-shaped POF with a thickness (d) of 600 μm.

Table 4 Experimental results of the LPGs with a period of 300 μm and different lengths imprinted on the flat-shaped POFs in Fig. 10 (D = 1 mm, d = 600 μm, and h = 200 μm).

Length L (cm)	δ	Sensitivity (%/RIU)	Resolution (RIU)	Correlation coefficient R^2
2	1.44×10^{-3}	450.7	9.585×10^{-4}	0.9959
4	2.64×10^{-3}	849.5	9.323×10^{-6}	0.9980
6	2.65×10^{-4}	1447	5.494×10^{-6}	0.9988

The 3 times repeated measurements were carried out under the same environmental conditions, and it showed that the repeatability and hysteresis errors of the sensor were limited, as shown in Fig. 11.

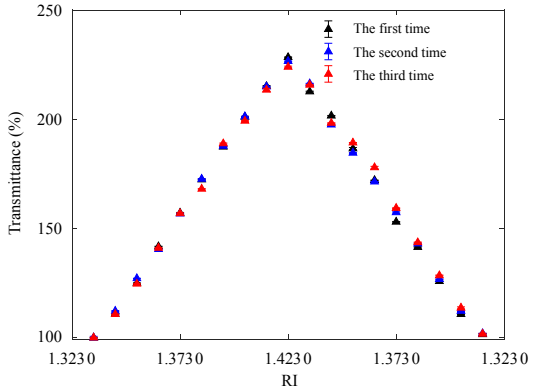

Fig. 11 Repetitive and hysteresis performance of the sensor, where the LPG period is 300 μm, the length is 6 cm, the groove depth is 200 μm, and the thickness (d) of the flat-shaped POF is 600 μm.

4. Influence of de-cladding, tilted LPG, and bending

After changing the thickness of the flat-shaped POF and parameters of the LPG (the period, groove depth, and length), the sensing probe was optimized. Therefore, for the LPG with a period of 300 μm, a groove depth of 200 μm, and a length of 6 cm imprinted on the flat-shaped POF, the influences of de-cladding the POF, tilting the LPG, and bending the device were tested, and the RI performance was also improved.

4.1 De-cladding

The cladding in the sensing section of the flat-shaped POF was removed by chemical etching [28], after that, an LPG was pressed on it. The RI sensing performances of the LPG imprinted on the flat-shaped POF, both with and without the cladding, are shown in Fig. 12. The experimental results of the LPG imprinted on the flat-shaped POF with or without the cladding in Fig. 12 are listed in Table 5. It showed that after the cladding was removed, the RI sensitivity of the sensor was improved from 1447%/RIU to 2250%/RIU.

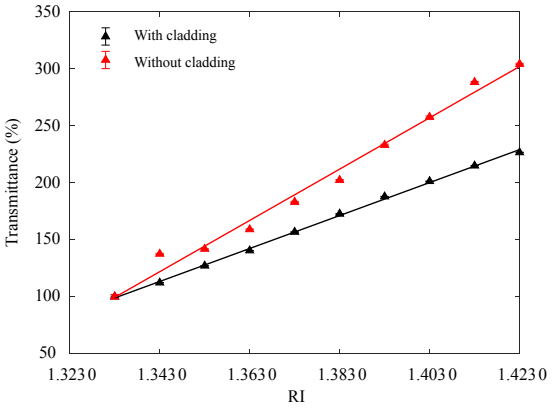

Fig. 12 RI sensing performances of the LPGs with a period length of 300 μm and a groove depth (h) of 200 μm imprinted on the flat-shaped POFs with and without the cladding. The thickness (d) of the flat-shaped POF is 600 μm and the length (L) of flat-shaped POF section is 6 cm.

Table 5 Experimental results of LPGs imprinted on the flat-shaped POFs with or without the cladding in Fig. 12 (D = 1 mm, d = 600 μm, h = 200 μm, and L = 6 cm).

POF	δ	Sensitivity (%/RIU)	Resolution (RIU)	Correlation coefficient R^2
With cladding	2.65×10^{-4}	1447	5.494×10^{-6}	0.9988
Without cladding	2.03×10^{-4}	2250	2.707×10^{-6}	0.9874

4.2 Tilted LPG

The tilted LPG was fabricated on the obtained flat-shaped POF with the thickness of 600 μm and length of 6 cm, as shown in Fig. 13, and the tilted LPGs with tilted angles of 0°, 15°, and 30° were fabricated. Among them, the period of the tilted LPG was 300 μm, and the groove depth was 200 μm. The RI sensing performances are shown in Fig. 14, which showed that the sensitivity increased as the tilted angle increased. When the tilted angle was 30°, the RI sensitivity reached 2367%/RIU. The experimental results at different tilted angles in Fig. 14 are listed in Table 6.

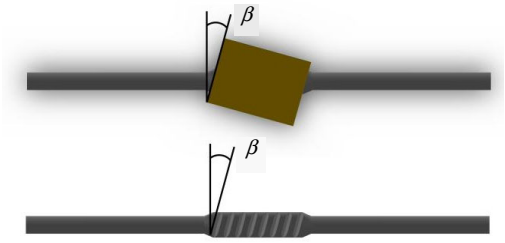

Fig. 13 Schematic diagram of a tilted LPG imprinted on a flat-shaped POF.

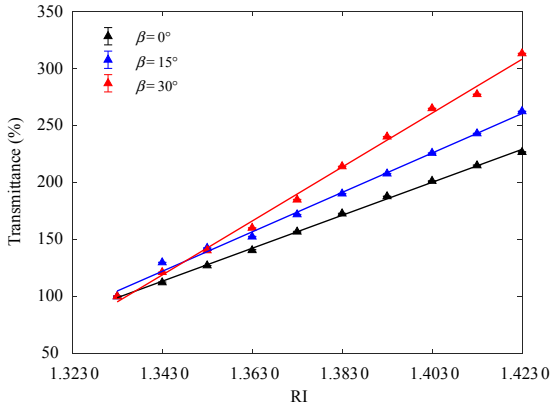

Fig. 14 RI sensing performances of LPGs with different tilted angles (β) imprinted on the flat-shaped POFs.

Table 6 Experimental results of LPGs with different tilted angles (β) imprinted on the flat-shaped POFs in Fig. 14 (D=1 mm, d=600 μm, h=200 μm, and L=6 cm).

Tilted angle β (°)	δ	Sensitivity (%/RIU)	Resolution (RIU)	Correlation coefficient R^2
0	2.65×10^{-4}	1447	5.494×10^{-6}	0.9988
15	6.14×10^{-5}	1731	1.064×10^{-7}	0.9952
30	4.03×10^{-5}	2367	5.108×10^{-8}	0.9957

4.3 Bending

The LPG with a period length of 300 μm and a groove depth of 200 μm imprinted on the flat-shaped POFs with a thickness of 600 μm and a length of 6 cm was bent at different curvature radii (r) by simple mechanical bending and fixing the two ends of the LPG, and the curvature radii (r) were $24/\pi$ cm, $12/\pi$ cm, $8/\pi$ cm, and $6/\pi$ cm, respectively. The schematic diagram of the bending structure is shown in Fig. 15. The RI sensing performance of the bending LPG imprinted on the flat-shaped POF is shown in Fig. 16, and it showed that the sensitivity increased as the curvature radium decreased. When the curvature radius was $6/\pi$ cm, the RI sensitivity reached 6 563%/RIU in the RI range of 1.3330–1.4230. The experimental results of the sensor at different bending angles in Fig. 16 are listed in Table 7.

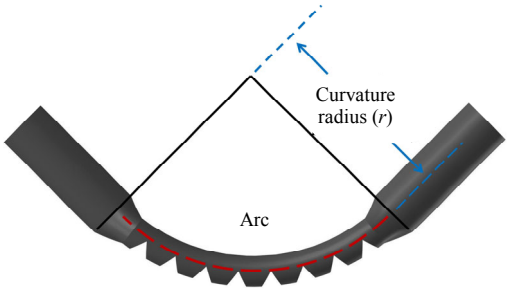

Fig. 15 Schematic diagram of the bending structure.

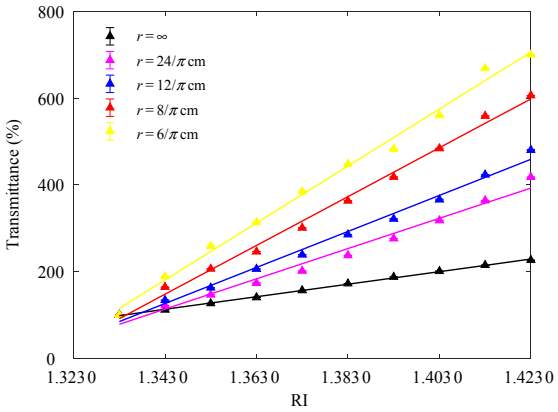

Fig. 16 RI sensing performances of LPGs imprinted on the flat-shaped POFs with different curvature radii (r).

Table 7 Experimental results of LPGs imprinted on the flat-shaped POFs with different curvature radii (r) in Fig. 15 (D = 1 mm, d = 600 μm, h = 200 μm, and L = 6 cm).

Curvature radius r (cm)	δ	Sensitivity (%/RIU)	Resolution (RIU)	Correlation coefficient R^2
∞	2.65×10^{-4}	1 447	5.494×10^{-6}	0.998 8
$24/\pi$	1.54×10^{-5}	3 485	1.326×10^{-8}	0.980 8
$12/\pi$	7.17×10^{-6}	4 152	5.181×10^{-9}	0.991 2
$8/\pi$	3.51×10^{-6}	5 626	1.872×10^{-9}	0.994 8
$6/\pi$	5.44×10^{-6}	6 563	2.487×10^{-9}	0.993 7

Finally, a comparison between the proposed RI sensor and the previously reported ones is summarized in Table 8.

Table 8 Comparison with previously reported POF RI sensors.

Sensor structure	RI measurement range	Sensitivity (%/RIU)	Resolution (RIU)	Ref.
Multi-notched POF	1.333–1.410	1 130	8.44×10^{-4}	[21]
POF with LPG structure	1.33–1.45	2 815	1.39×10^{-4}	[22]
D-shaped POF with LPG structure	1.33–1.45	2 676 (1.33–1.40)	4.17×10^{-5}	[23]
		9 786 (1.40–1.45)	1.14×10^{-5}	
		2 277 (1.33–1.37)	3.10×10^{-4}	
Twisted tapered POF	1.37–1.44	1 700 (1.37–1.41)	–	[24]
		3 496 (1.41–1.44)		
Screw-shaped POF	1.33–1.45	4 318 (1.37–1.40)	1.63×10^{-4}	[25]
		4 399 (1.41–1.45)	1.60×10^{-4}	
Flat-shaped POF with LPG	1.333 0–1.423 0	2 367 (straight) 6 563 (bending)	5.108×10^{-8} 2.487×10^{-9}	This work

5. Conclusions

In this work, an LPG imprinted on a flat-shaped POF was proposed as an RI sensor. A simple pressing with the heat pressure and mechanical die press print method was carried out to modify the structure of POFs for RI sensing enhancement. It was mainly made by the following two steps: the commercial POF was firstly pressed with the heat pressure to form a flat-shaped POF, and then, the LPG was formed on the surface of the obtained flat-shaped POF by the method of the mechanical die press print. The influences of the thickness of the flat-shaped structure, the groove depth, and the length of the LPG over the RI measurement were investigated theoretically and experimentally. The experimental results showed that the sensor with a thinner flat thickness, a longer length, and a deeper groove depth of the corrugated surface LPG exhibited the better RI sensing performance, which coincided with the theoretical calculation results. By choosing that the thickness of the flat-shaped POF with the cladding was 600 μm, the LPG period was 300 μm, the groove depth was 200 μm, and the length was 6 cm, the RI sensitivity of 1 447%/RIU was obtained in the RI range of 1.333 0–1.423 0. In addition, the influences of de-cladding the POF, tilting the LPG, and bending the sensing structure on the sensitivity of RI were investigated. The results demonstrated that the RI sensitivity of the sensor after removing the cladding of the POF, tilting the LPG, or bending the LPG was better than that of the original one. When the curvature radius of the LPG imprinted on the flat-shaped POF was $6/\pi$ cm, the highest sensitivity of 6 563%/RIU was achieved in the range of 1.333 0–1.423 0.

Declarations

Conflict of Interest The authors declare that they have no competing interests.

References

[1] J. Lou, Y. Wang, and L. Tong, "Microfiber optical sensors: a review," *Sensors*, 2014, 14(4): 5823–5844.

[2] A. Tapetado, P. J. Pinzón, J. Zubia, and C. Vázquez, "Polymer optical fiber temperature sensor with dual-wavelength compensation of power fluctuations," *Journal of Lightwave Technology*,

2015, 33(13): 2716–2723.

[3] C. Teng, H. Liu, H. Deng, S. Deng, H. Yang, R. Xu, *et al.*, "Liquid level sensor based on a V-groove structure plastic optical fiber," *Sensors*, 2018, 18(9): 3111.

[4] N. Jing, C. Teng, J. Zheng, G. Wang, Y. Chen, and Z. Wang, "A liquid level sensor based on a race-track helical plastic optical fiber," *IEEE Photonics Technology Letters*, 2016, 29(1): 158–160.

[5] C. Teng, S. Deng, H. Deng, H. Yang, Y. Xu, L. Yuan, *et al.*, "Investigation of a plastic optical fiber imprinted with V-groove structure for displacement sensing," *Optical Engineering*, 2019, 58(7): 072002.

[6] P. Fabbri, F. Pilati, L. Rovati, R. McKenzie, and J. Mijovic, "Poly(ethylene oxide)-silica hybrids entrapping sensitive dyes for biomedical optical pH sensors: molecular dynamics and optical response," *Optical Materials*, 2011, 33(8): 1362–1369.

[7] G. Durana, M. Kirchhof, M. Luber, I. Sáez de Ocáriz, H. Poisel, J. Zubia, *et al.*, "Use of a novel fiber optical strain sensor for monitoring the vertical deflection of an aircraft flap," *IEEE Sensors Journal*, 2009, 9(10): 1219–1225.

[8] A. G. Leal-Junior, A. Theodosiou, C. R. Diaz, C. Marques, M. J. Pontes, K. Kalli, *et al.*, "Simultaneous measurement of axial strain, bending and torsion with a single fiber Bragg grating in CYTOP fiber," *Journal of Lightwave Technology*, 2018, 37(3): 971–980.

[9] R. Min, Z. Liu, L. Pereira, C. Yang, Q. Sui, and C. Marques, "Optical fiber sensing for marine environment and marine structural health monitoring: a review," *Optics & Laser Technology*, 2021, 140: 107082.

[10] R. Khan, B. Gul, S. Khan, H. Nisar, and I. Ahmad, "Refractive index of biological tissues: review, measurement techniques, and applications," *Photodiagnosis and Photodynamic Therapy*, 2021, 33: 102192.

[11] X. Yan, H. Li, and X. Su, "Review of optical sensors for pesticides," *TrAC Trends in Analytical Chemistry*, 2018, 103: 1–20.

[12] Y. Chen, J. Liu, Z. Yang, J. S. Wilkinson, and X. Zhou, "Optical biosensors based on refractometric sensing schemes: a review," *Biosensors and Bioelectronics*, 2019, 144: 111693.

[13] K. Schroeder, W. Ecke, R. Mueller, R. Willsch, and A. Andreev, "A fibre Bragg grating refractometer," *Measurement Science and Technology*, 2001, 12(7): 757–764.

[14] T. Chuanxin, P. Shao, R. Min, H. Deng, M. Chen, S. Deng, *et al.*, "Simultaneous measurement of refractive index and temperature based on a side-polish and V-groove plastic optical fiber SPR sensor," *Optics Letters*, 2023, 48(2): 235–238.

[15] H. J. Patrick, A. D. Kersey, and F. Bucholtz, "Analysis of the response of long period fiber gratings to external index of refraction," *Journal of Lightwave Technology*, 1998, 16(9): 1606–1612.

[16] F. Yu, P. Xue, and J. Zheng, "Enhancement of refractive index sensitivity by bending a core-offset in-line fiber Mach-Zehnder interferometer," *IEEE Sensors Journal*, 2019, 19(9): 3328–3334.

[17] C. Teng, R. Min, J. Zheng, S. Deng, M. Li, L. Hou, *et al.*, "Intensity-modulated polymer optical fiber-based refractive index sensor: a review," *Sensors*, 2022, 22(1): 81.

[18] C. Teng, N. Jing, F. Yu, and J. Zheng, "Investigation of a macro-bending tapered plastic optical fiber for refractive index sensing," *IEEE Sensors Journal*, 2016, 16(20): 7521–7525.

[19] N. Jing, J. Zheng, X. Zhao, and C. Teng, "Investigation of a macrobending micro-plastic optical fiber for refractive index sensing," *Applied Optics*, 2014, 53(34): 8145–8150.

[20] N. Jing, J. Zheng, X. Zhao, and C. Teng, "Refractive index sensing based on a side-polished macrobending plastic optical fiber," *IEEE Sensors Journal*, 2014, 15(5): 2898–2901.

[21] C. Teng, N. Jing, F. Yu, Y. Ding, and J. Zheng, "Refractive index sensor based on a multi-notched plastic optical fiber," *Applied Optics*, 2017, 56(7): 1833–1838.

[22] P. Xue, F. Yu, Y. Cao, and J. Zheng, "Refractive index sensing based on a long period grating imprinted on a multimode plastic optical fiber," *IEEE Sensors Journal*, 2019, 19(17): 7434–7439.

[23] P. Xue, F. Yu, B. Wu, H. Bao, and J. Zheng, "Investigation of a D-shaped plastic optical fiber assisted by a long period grating for refractive index sensing," *IEEE Sensors Journal*, 2020, 20(2): 842–847.

[24] C. Teng, H. Deng, H. Liu, H. Yang, L. Yuan, J. Zheng, *et al.*, "Refractive index sensor based on twisted tapered plastic optical fibers," *Photonics*, 2019, 6(2): 40.

[25] P. Xue, B. Wu, H. Bao, and J. Zheng, "Screw-shaped plastic optical fibers for refractive index sensing," *IEEE Sensors Journal*, 2020, 20(10): 5237–5242.

[26] M. S. Kovacevic, A. Djordjevich, and D. Nikezic, "Analytical optimization of optical fiber curvature gauges," *IEEE Sensors Journal*, 2008, 8(3): 227–232.

[27] H. Bao, B. Wu, Y. Liu, Y. Zhou, and J. Zheng, "Investigation of long period grating imprinted on a plastic optical fiber for liquid level sensing," *Optik*, 2022, 251: 168367.

[28] S. Grassini, M. Ishtaiwi, M. Parvis, and A. Vallan, "Design and deployment of low-cost plastic optical fiber sensors for gas monitoring," *Sensors*, 2014, 15(1): 485–498.